Available online at www.sciencedirect.com
SCIENCE DIRECT®
Biomaterials 27 (2006) 2627–2636
Biomaterials
www.elsevier.com/locate/biomaterials

Fabrication and characterization of heparin functionalized membrane-mimetic assemblies

Po-Yuan Tseng[a], Shyam M. Rele[b], Xue-Long Sun[b], Elliot L. Chaikof[a,b,*]

[a]*School of Chemical Engineering, Georgia Institute of Technology, Atlanta, GA 30320, USA*
[b]*Laboratory for Biomaterials and Tissue Engineering, Departments of Surgery and Biomedical Engineering, Emory University School of Medicine, Atlanta, GA 30322, USA*

Received 24 July 2005; accepted 29 October 2005
Available online 20 December 2005

Abstract

A membrane-mimetic assembly incorporating surface bound heparin was fabricated as a system to improve the hemocompatibility of blood-contacting devices. As a model system, heparin was chemically modified by end-point conjugation to biotin and immobilized onto membrane-mimetic thin films via biotin–streptavidin interactions. Heparin surface density, determined by radiochemical titration, confirmed that surface density was directly related to the molar concentration of biotinylated lipid within the assembled membrane-mimetic film. The capacity of surface bound heparin to promote ATIII-mediated thrombin inactivation was investigated in a parallel plate flow chamber under simulated venous and arterial wall shear rates of 50 and 500 s^{-1}, respectively. Significantly, we observed that the rate of thrombin inactivation approached a maximum at a heparin surface concentration greater than 4.4 pmol/cm^2 (61 ng/cm^2). In the process, mass transport limited regimes were identified for heparin potentiated thrombin inactivation under both simulated venous and arterial conditions.

Keywords: Anticoagulant; Biomimetics; Heparin; Antithrombogenic; Membrane-mimetic

1. Introduction

Clinically used since 1930s [1], heparin is the most common anticoagulant for preventing blood clotting during surgery and in the treatment of postoperative thrombosis and embolism. Pharmacologically, the well-known anticoagulant activity of heparin is predominantly due to its ability to accelerate the rate by which antithrombin III (ATIII) inactivates thrombin, factor Xa, and factor IXa [2,3]. This effect is mediated through an unique pentasaccharide sequence, which induces a conformational change in antithrombin that increases the rate of target proteinase inhibition by 2000- to 4000-fold in the presence of optimal heparin concentration [4–9].

Heparinization of artificial surfaces has been shown to be a successful strategy to prevent thrombus formation and improve the hemocompatibility of blood-contacting surfaces. In general, binding of ATIII is most efficient when heparin is coupled by end-point attachment. For example, covalent bonding of nitrite-degraded heparin onto membrane oxygenators and tubings by end-point attachment has made it possible to maintain a long-lasting extracorporeal circulation without systemic heparinization [10]. Moreover, heparin activity appears to be further enhanced when coupled to a surface via a spacer arm. In this regard, heparin immobilized through poly(ethylene oxide) (PEO) spacer groups onto polyurethane surfaces has consistently enhanced bioactivity when evaluated using in vitro, ex vivo, and in vivo test systems [11,12]. Further, other investigators have demonstrated that when linked to a substrate via an alkyl group, heparin activity is enhanced with increasing length of the spacer arm [13]. Detailed investigations have revealed that spacer arm-immobilized heparin acts by initially binding antithrombin, which is followed by the formation of a ternary complex with thrombin [14,15].

*Corresponding author. 101 Woodruff Circle 5105 WMB, Emory University, Atlanta, GA 30322, USA. Tel.: +1 404 727 8413; fax: +1 404 727 3660.
E-mail address: echaiko@emory.edu (E.L. Chaikof).

0142-9612/$ - see front matter © 2005 Elsevier Ltd. All rights reserved.
doi:10.1016/j.biomaterials.2005.10.032

We have previously proposed that membrane-mimetic thin films provide a convenient platform for improving the clinical performance of blood-contacting artificial organs and other implantable medical devices by modulating maladaptive processes at both blood–material and tissue–material interfaces [16–21]. Specifically, we believe that the self-assembly of polymerizable lipids in association with transmembrane proteins [16], as well as peptide or carbohydrate lipophilic conjugates establishes a versatile scheme for generating chemically heterogeneous films with tailored biological functionality [17]. As such, we have recently reported the synthesis of a membrane-mimetic thin film composed of mixed polymerizable lipids containing both phosphatidylcholine and biotin headgroups [17,22]. This has allowed us to fabricate a series of model membrane-mimetic films that have been derivatized at varying surface densities with chain end terminated biotinylated heparin (Fig. 1). In the process of generating these model heparinized membrane-mimetic thin films, we examined heparin potentiated thrombin inactivation under simulated venous ($50\,s^{-1}$) and arterial ($500\,s^{-1}$) flow conditions.

2. Experimental methods

2.1. Materials

Human thrombin and ATIII were obtained from Haematologic Technologies, Inc. Heparin (sodium salt, porcine intestinal mucosa, Mw: 12–14 kDa) and streptavidin (SA) were obtained from Calbiochem. Biotin and polybrene (1,5-dimethyl-1,5-diazaundecamethylene polymethobromide) were obtained from Sigma. Tritiated heparin was purchased from Perkin Elmer. Chromogenic substrate for thrombin Spectrozyme TH: H-D-hexahydrotyrosyl-L-alanyl-L-arginine-*p*-nitroanilide-diacetate salt was purchased from American Diagnostica. Eosin Y (EY, 5% in water), triethylamine (TEA), 1-vinyl-2-pyrrolidinone (VP) were obtained from Aldrich. Nucleopore polycarbonate filters, circular glass coverslips (12 mm diameter, 0.17 mm thickness) and Contrad 70 detergent were obtained from Fisher. Alginate (ALG; low viscosity, ca. 60% mannuronic acid) was obtained from Pronova Biomedical. Poly(L-lysine) (PLL, Mw > 300 kDa) and all buffer salts were obtained from Sigma. Synthesis of monoacrylate-PC (AcPC, 1-palmitoyl-2-[12-(acryloyloxy)dodeca-noyl]-*sn*-glycero-3-phosphocholine), monoacrylate-PE (AcPE, 1-palmitoyl-2-(12-(acryloyloxy)dodecanoyl)-*sn*-glycero-3-phosphoethanolamine) and its biotin derivative (biotin-AcPE, mono-acrylPE-biotin) have been described previously [21,22]. The synthesis of a terpolymer that consists of (3-acryloyl-3-oxapropyl-3-(*N*,*N*-dioctadecyl-carbamoyl)-propionate))$_6$:(2-hydroxyethyl acrylate)$_3$:sodium styrene sulfonate$_1$ (AOD_6:HEA_3:SS_1) has been detailed elsewhere [19].

2.2. Instrumentation

Biotinylated heparin was characterized by NMR spectroscopy for component analysis and size exclusion chromatography/laser light scattering (SEC/LLS) to determine molecular weight and polydispersity. ^{1}H NMR spectra were recorded on Varian INOVA 400 MHz or 600 MHz NMR spectrometers. For ^{1}H NMR spectra recorded in $CDCl_3$, D_2O and CD_3OD chemical shifts (δ) are given in ppm relative to solvent peaks ($CDCl_3$ ^{1}H $\delta = 7.26$, D_2O ^{1}H $\delta = 4.85$, CD_3OD ^{1}H $\delta = 4.87$ & 3.32) as an internal standard. Coupling constants (J) are reported in Hertz (Hz). ^{3}H-labeled materials were detected using a scintillation counter (Beckman LS

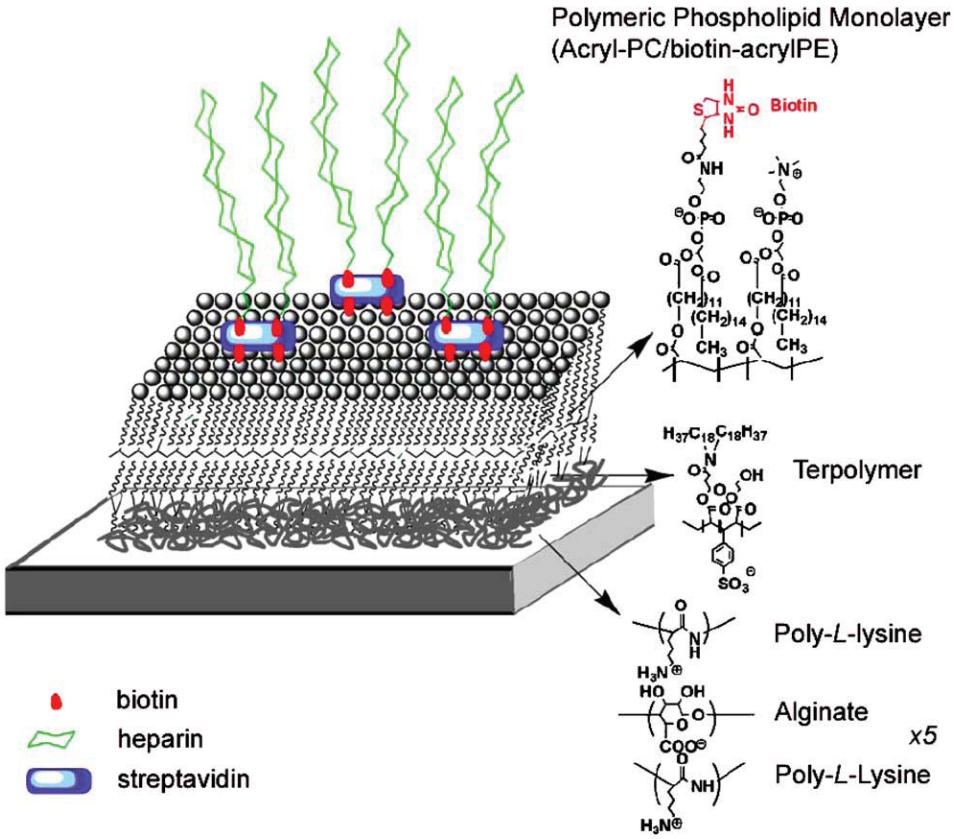

Fig. 1. Schematic representation of immobilized heparin on a polymeric phospholipid monolayer supported on an alkylated polyelectrolyte thin film (not to scale).

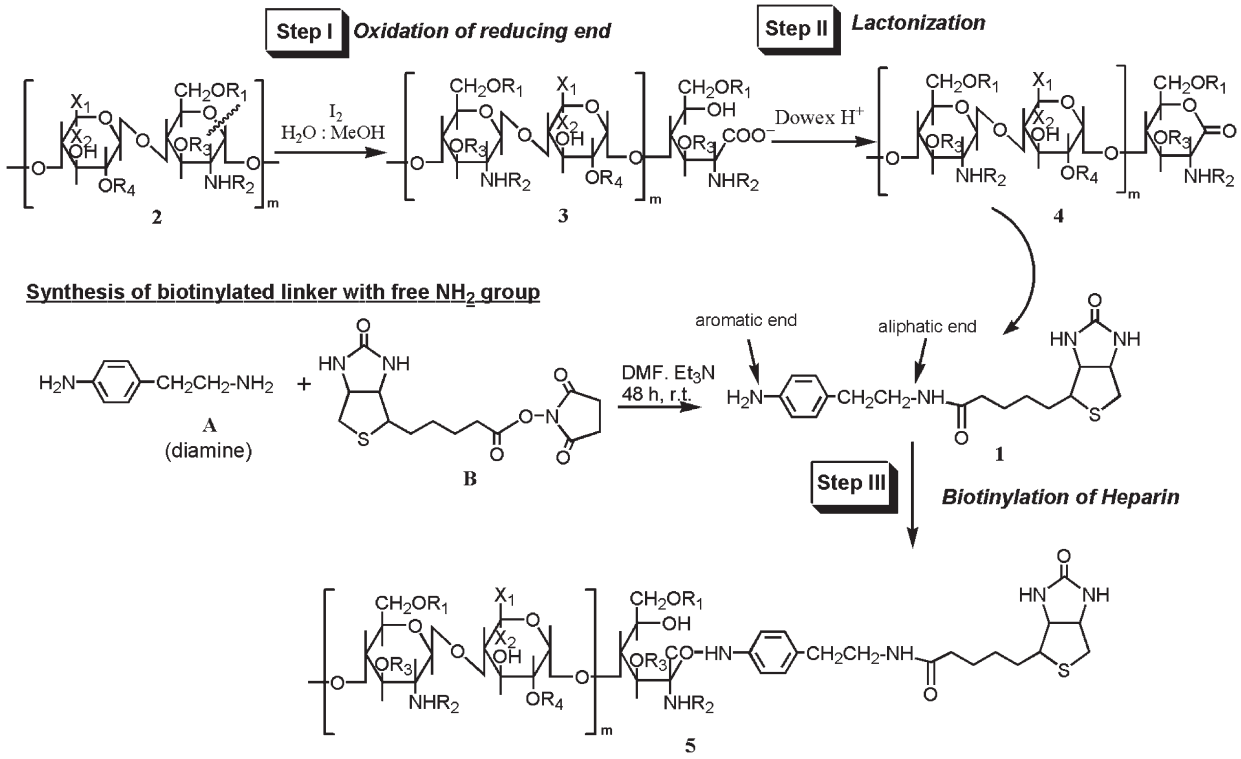

Fig. 2. Scheme for the synthesis of biotin chain terminated heparin.

6000IC). UV-Visible spectrophotometric measurements were executed on a Cary 50 Bio spectrophotometer (Varian) equipped with a temperature-regulated cell compartment.

2.3. Synthesis and characterization of biotin-conjugated heparin

The procedure for preparation of biotinylated heparin is illustrated in Fig. 2. The synthetic strategy is divided in two parts: (i) generation of biotinylated linker with free amine; and (ii) preparation of end group functionalized heparin lactone capable of reacting with the free amine. Synthesis of biotinylated linker **1** was achieved by reacting 2-(4-aminophenyl) ethylamine (**A**) with *N*-biotin succinimide (**B**). In order to obtain the targeted bioconjugate, heparin **2** was oxidized using I_2. This resulted in the cleavage of C–O bond of the glucopyranose ring at the reducing end of heparin affording **3** with a free hydroxyl and carboxylate group. Passage of **3** through a Dowex H^+ ion exchanger column resulted in lactonization affording **4**. Subsequent reaction of the lactone with the designed biotinylated free amine derivative **1** furnished the desired product (biotinylated heparin **5**), which was then dialyzed, lyophilized, chromatographed using Sephadex G-25 (water as eluant) and purified using the ImmunoPure™ Immobilized Monomeric Avidin kit (Pierce). A HABA (4-hydroxyazobenzene-2-carboxylic acid) assay (Sigma) was used to determine the moles of biotin per mole of heparin [23]. Molecular weight and polydispersity of **5** were 13.8 kDa and 1.115, respectively, by SEC/LLS analysis (Table 1). HABA assay revealed that the extent of biotinylation was 0.92 ± 0.03 mol of biotin/mol heparin.

2.3.1. Preparation of amine terminated biotin linker *1*

Triethyl amine (Et_3N, 1.25 eq., 3.662 mmol, 510 μL) was added to a solution of 2-(4-aminophenyl)-ethylamine **A** (1.2 eq., 3.51 mmol, 478 mg) in dry DMF and the solution was stirred at room temperature for 20 min under an Argon atmosphere. To this mixture, *N*-biotin succinimide **B** (2.93 mmol, 1.0 g) dissolved in DMF was added and the reaction was allowed to stir at room temperature for 24 h. Removal of the solvent under vacuum afforded a residue, which was purified by silica gel column chromatography using 10% $CHCl_3$ + MeOH mixture as the eluent. The expected product **1** was isolated as a pale yellow solid, which was confirmed by NMR analysis (Fig. 3). ^{1}H NMR of **1** (400 MHz, 9:1 CD_3OD:$CDCl_3$) δ 6.93 (d, 2H, $J = 5.6$ Hz), 6.63 (d, 2H, $J = 5.6$ Hz), 4.43 (dd, 1H, $J = 3.2$ Hz, NH-CH), 4.21 (m, 1H, $J = 3.2$ Hz, NH-CH), 3.1 (m, 1H, S-CH), 2.86 (dd, 1H, $J = 3.2$ Hz), 2.67–2.59 (5H, Ar-CH_2 + NH-CH_2 + S-CH), 2.09 (t, 2H, $J = 4.4$ Hz, CO-CH_2), 1.68–1.52 (m, 4H, $(CH_2)_2$), 1.15 (m, 2H, CH_2).

Table 1
Polydispersity and molecular weight of heparin and biotin–heparin

	Polydispersity index (PDI)	Molar mass moments (g/mol)	
		Mw (kDa)	Mz (kDa)
Heparin	1.084	14.3	15.1
Biotin–heparin	1.115	13.8	15.3

2.3.2. Preparation of heparin–lactone *4*

Heparin sodium salt **2** was dissolved in water and passed through the protonated Dowex resin (50×8 H^+) and eluted with water. The eluate was dialyzed and lyophilized to obtain heparin in protonated form. Heparin–lactone was prepared by oxidizing the reducing end of the protonated heparin (0.0392 mmol, 550 mg) by iodide (20 eq.) in 20% aqueous MeOH solution (100 mL) for 6–8 h at room temperature. On completion of the oxidation process, as assessed by the 3,5-dinitrosalicylcic acid method, the reaction solution was poured into an 4% ethanolic KOH solution (100 mL). The mixture was allowed to stand for 30–45 min and then the supernatant solution was centrifuged and decanted. A white residue was obtained, dissolved in water, and subjected to dialysis

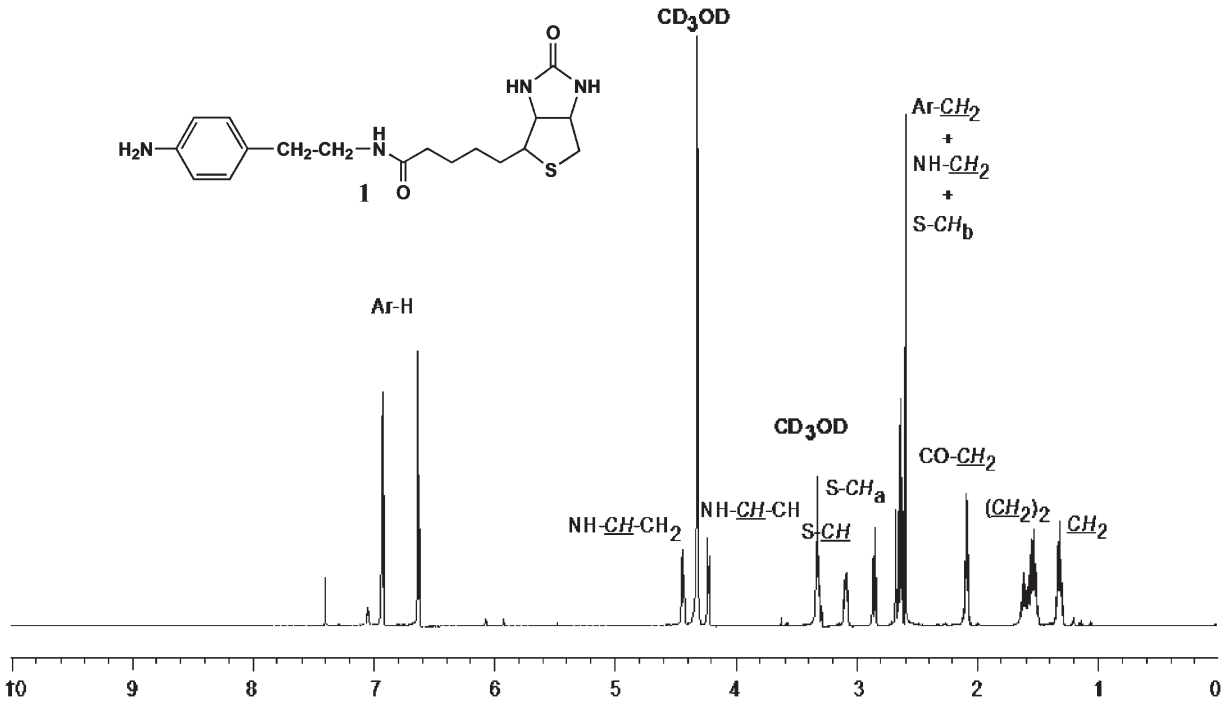

Fig. 3. ^{1}H NMR spectrum of amine terminated biotin spacer arm **1**.

(MWCO ~3500) for 24 h. The sample solution was freeze dried and lyophilized to obtain the oxidized heparin product **3** (Yield: 370 mg). Compound **3** was subsequently dissolved in distilled water and passed through a protonated Dowex resin (50 × 8 H^+) and stirred for 30 min. The eluant was then filtered and washed with water several times to ensure the complete removal of **4** from the resin. The sample solution was freeze dried and lyophilized to obtain the heparin–lactone **4** (Yield: 300 mg). Though NMR could not determine the purity of the lactone, size exclusion chromatography/laser light scattering (SEC/LLS) analyses before and after the modification showed that there was little significant change between the GPC pattern of lactone and heparin, indicating that oxidative cleavage of the main backbone did not occur.

2.3.3. Preparation of biotinylated heparin 5

Amine terminated biotin **1** (10 eq., 0,22 mmol, 75 mg) dissolved in DMF was added to a solution of heparin–lactone **4** (0.022 mmol, 300 mg) in DMF containing diisopropylethylamine (10 eq., 40 μL). The reaction mixture was stirred for 8 h at 55–60 °C, concentrated under vacuum, and washed with $CHCl_3$/MeOH mixture to remove the excess aminated biotin. The crude residue was dissolved in water, dialyzed (36 h, MWCO ~3500), and freeze dried to obtain the desired biotinylated heparin **5**, which was purified by gel permeation chromatography (Sephadex G-25) using water as an eluant. The water fractions containing the product were pooled, lyophilised and purified using ImmunoPure^{TM} Immobilized Monomeric Avidin kit to afford a pale yellow biotin-functionalised heparin derivative **5**. Yield: 180 mg (60%). The final product was confirmed by NMR analysis (Fig. 4). ^{1}H NMR of **5** (600 MHz, D_2O) δ 7.6–7.2 (m, ArH), 5.72–4.91 (m, ring protons), 4.75–4.1 (m, ring protons + NH-CH), 4.08–3.35 (m, ring protons), 3.06–2.76 (m, Ar-CH_2 + NH-CH_2 + S-CH), 2.09 (s, CO-CH_2), 2.01 (s, NH-Ac), 1.6–1.2 (m, $(CH_2)_n$ protons). Molecular weight and polydispersity were characterized by SEC/LLS analysis (Table 1).

2.4. Analysis of biotin–heparin activity

Heparin activity was defined by its capacity to inactivate thrombin by antithrombin. Briefly, HEPES buffer (20 mM HEPES + 100 mM NaCl + 0.5 wt% BSA) containing heparin was incubated with 10 nM human ATIII at 37 °C for 5 min, followed by the addition of 10 nM human thrombin. At timed intervals, aliquots were withdrawn and added to Tris buffer (50 mM Tris–HCl + 175 mM NaCl + 0.05 wt% BSA, pH 7.9) containing 1 mg/mL Polybrene [24,25] and chromogenic substrate Spectrozyme TH (0.2 mM final). Residual thrombin was determined by UV-VIS spectroscopy and a standard curve.

2.5. Fabrication of biotin-functionalized membrane-mimetic thin films

2.5.1. Preparation of a (PLL-ALG)$_5$-PLL-terpolymer film

Glass coverslips were cleaned by 30 min of sonication in 10% Contrad 70 detergent solution followed by extensive washing and sonication in deionized water. PLL and ALG were prepared at concentrations of 0.10 and 0.15 w/v% in phosphate-buffered saline (PBS; 20 mM NaH_2PO_4, 0.9 w/v% NaCl, pH 7.4), respectively. Cleaned substrates were then coated with PLL and ALG alternating monolayers to form 11 layers (six PLL and five alginate layers), with the top layer comprised of PLL. The (PLL-ALG)$_5$-PLL-coated substrates were then exposed to a 0.1 mM solution of terpolymer (AOD_6:HEA_3:SS_1) dissolved in a mixture of 20 mM NaH_2PO_4/DMSO (99:1 v/v), pH 7.4 for 90 s. The (PLL-ALG)$_5$-PLL-terpolymer-coated samples were then rinsed 7–10 times with deionized water.

2.5.2. Vesicle fusion

Large unilamellar vesicles (LUVs) totaling 12 mM lipid (in either 0, 2, 5, 10, 20, or 50 mol% biotin-AcPE) in 20 mM sodium phosphate buffer (pH 7.4) were prepared by four successive freeze/thaw/vortex cycles using liquid N_2 and a 65 °C water bath. The LUVs were then extruded 21 times each through 2.0 and 0.6 μm polycarbonate filters (Millipore), and the solution diluted to 1.2 mM with 20 mM sodium phosphate buffer (pH 7.4) and 150 mM NaCl. The (PLL-ALG)$_5$-PLL-terpolymer-coated substrates were then incubated with the vesicle solution at 43 °C for 14–16 h.

2.5.3. In situ photopolymerization of a supported lipid film

Details of the photopolymerization of lipid films on alkylated glass and silicon substrates have been reported elsewhere [19,20]. Briefly, a stock

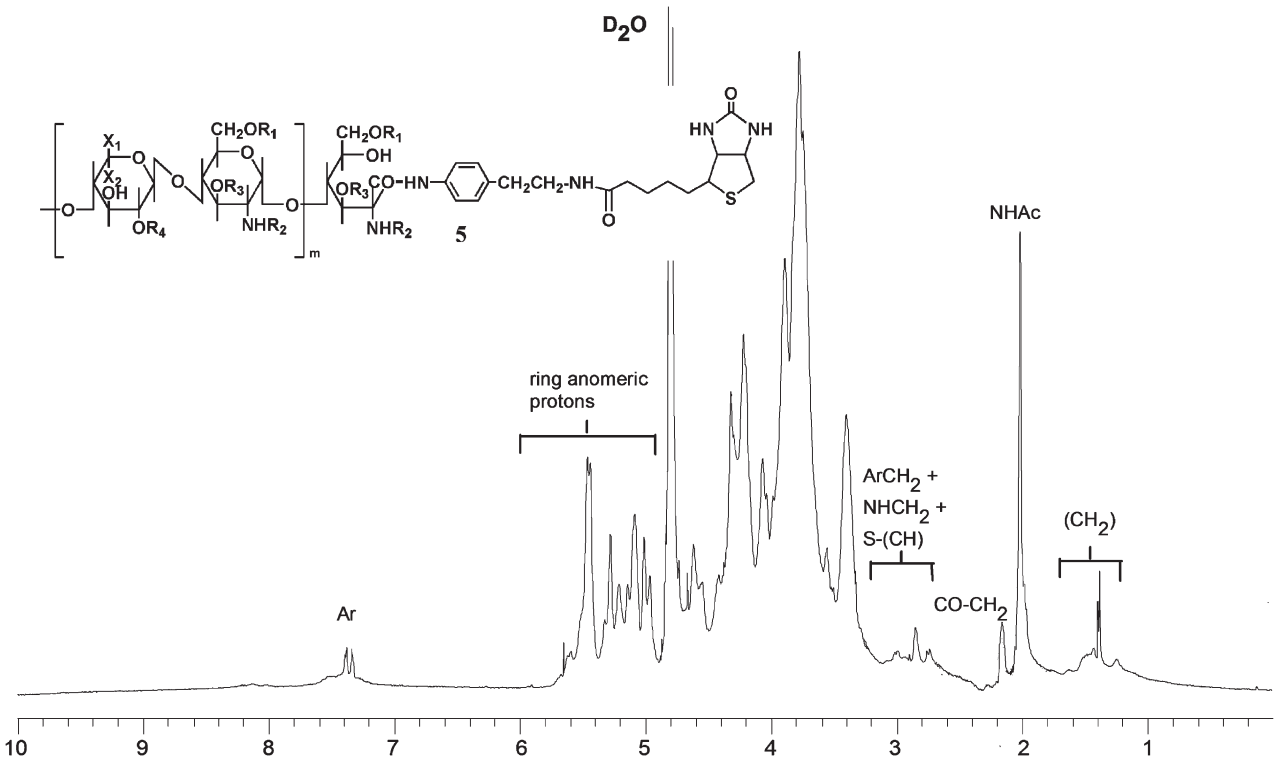

Fig. 4. ^{1}H NMR spectrum of biotin-functionalized heparin **5.**

solution of coinitiators was prepared as 10 mM EY, 225 mM triethanolamine (TEA), and 37 mM VP in water. A 10:1 (mol/mol) monomer/EY ratio was used for photopolymerization. After lipid fusion, the samples were placed into an Ar-purged atmosphere at 30% relative humidity and 10 μL of initiator was added per 1 mL of sample solution. The initiator was gently mixed by slowly rotating the vial in a horizontal circular motion without lifting it from the bench surface. The sample was then irradiated with a Dynalume visible light lamp at an intensity of approximately 40 mW/cm^2. Following photopolymerization, the samples were washed with deionized water 6–8 times.

2.6. Fabrication of a heparinized membrane-mimetic thin film

Streptavidin (SA) was prepared in PBST (50 mM NaH_2PO_4 and 150 mM NaCl, pH 7.4) at a concentration of 5 μg/mL and incubated for 15 min on a horizontal rotating platform with biotinylated films, followed by extensive (~10 ×) rinsing with deionized water. SA-coated lipid membranes were then incubated with biotin-conjugated heparin **5** (0.1 mg/mL) prepared in PBST for 12–14 h at 4 °C on a horizontal rotating platform. The membrane was then rinsed extensively (~10 ×) with deionized water.

2.7. Determination of heparin surface density

^{3}H-heparin and unlabeled heparin were mixed to form a mass ratio of 1:160 for biotinylation, as described previously. The biotinylated compound was purified using ImmunoPure® Immobilized Monomeric Avidin and specific activity (cpm/μg or cpm/pmol) of ^{3}H-heparin determined. Heparin surface density was characterized by incubating SA-coated membrane-mimetic thin films with ^{3}H-heparin for 12–14 h at 4 °C. Heparin surface density (pmol/cm^2) was calculated as cpm/specific activity/sample area). Test samples were fabricated as six replicates for each lipid composition.

2.8. Parallel plate flow assay

Heparinized surfaces were fabricated on a glass slide (2.6 cm × 4.6 cm, Fisher) by anchoring biotinylated heparin onto a SA-coated membrane-mimetic thin film, as described above. In order to vary heparin surface density, 5, 10, 20, and 50 mol% of biotin-AcPE membrane-mimetic surfaces were prepared for heparinization. Surface heparin activity was investigated under unidirectional flow conditions at shear rates 50 and 500 s^{-1}. A parallel plate flow system (0.6 cm (width) × 0.01 cm (height) × 3.6 cm (length), 22 μL volume) containing test samples was flushed with 20 mM HEPES buffer for 1 h at γ_w 2000 s^{-1} prior to performing the thrombin inactivation assay. The reaction was initiated by simultaneous perfusion with HBSA (20 mM HEPES + 190 mM NaCl + 0.05 wt% BSA, pH 7.5) [26] containing equimolar concentrations of thrombin (30 nM) and antithrombin (30 nM) at 37 °C. At pre-selected timed points, aliquots were withdrawn from the outlet of the reactor and assayed by adding to Tris buffer/EDTA (50 mM Tris–HCl + 175 mM NaCl + 0.05 wt% BSA + 20 mM EDTA, pH 7.9) containing Spectrozyme TH substrate (0.2 mM final) [26]. Residual thrombin concentration was determined by UV-VIS spectroscopy.

3. Results and discussion

3.1. Analysis of biotin–heparin activity

The capacity of biotinylated heparin to inactivate thrombin by ATIII was analyzed. Thrombin decay was dependent on the concentration of heparin or biotinylated heparin (b–H, **5**) in the range of 1 nM to 1 μM. A linear relationship between the reciprocal of the residual thrombin concentration and incubation time was observed and the kinetic analysis demonstrated that thrombin decay fits

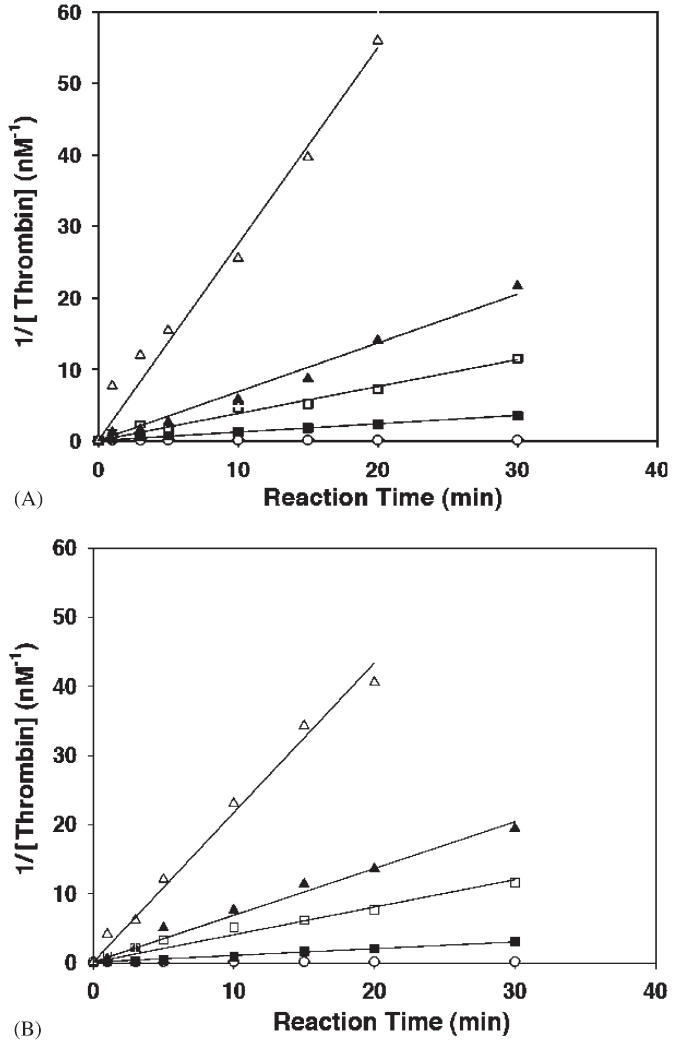

Fig. 5. Thrombin inactivation by antithrombin III in the presence of heparin (A) or biotin–heparin (B). Results for heparin concentrations ranging from 0 nM to 1 μM are presented: 0 nM (○), 10 nM (■), 40 nM (□), 0.1 μM (▲), and 1 μM (Δ). Each data point represents a mean value at each reaction time point ($n = 4$). Standard error was <10%.

a second–order reaction (Fig. 5) [9]. The slope of the curve represents the second–order rate constant (k_{app}) and little difference noted between heparin and the biotin–heparin conjugate (Table 2).

It was postulated that the predominant reaction mechanisms included direct inactivation of thrombin by ATIII, formation of heparin–ATIII complex, and inactivation of thrombin by the heparin–ATIII complex. In the heparin concentration range of 1 nM to 1 μM, we assumed that heparin–thrombin complex formation would be negligible [27]:

$$\mathrm{ATIII} + \mathrm{T} \xrightarrow{k_0} \mathrm{ATIII{-}T},$$

k_0 : 2nd-order rate constant without heparin,

$$\mathrm{b{-}H{-}ATIII} + \mathrm{T} \xrightarrow{k} \mathrm{ATIII{-}T} + \mathrm{b{-}H},$$

k : 2nd-order rate constant with heparin,

Table 2
Apparent second-order rate constants (k_{app}) for heparin and biotin–heparin

Concentration		Heparin	Biotin–heparin
μg/mL	μM	k_{app} ($M^{-1}\,min^{-1}$)	k_{app} ($M^{-1}\,min^{-1}$)
14	1	$(2.69\pm0.30)\times10^9$	$(2.01\pm0.38)\times10^9$
1.4	0.1	$(7.11\pm0.99)\times10^8$	$(6.50\pm0.14)\times10^8$
0.56	0.04	$(3.58\pm0.81)\times10^8$	$(3.13\pm0.32)\times10^8$
0.14	0.01	$(1.08\pm0.30)\times10^8$	$(1.03\pm0.24)\times10^8$
0.014	0.001	$(2.87\pm0.12)\times10^7$	$(6.87\pm1.88)\times10^6$
0	0	$(2.20\pm0.46)\times10^6$	$(2.20\pm0.46)\times10^6$

$$\mathrm{b{-}H} + \mathrm{ATIII} \overset{K_{HI}}{\leftrightarrow} \mathrm{b{-}H{-}ATIII},$$

K_{HI} : the dissociation constant of the b−H−ATIII complex.

The apparent rate constant k_{app} is a function of k_0, k, K_{HI}, and C_{b-H} [9]:

$$k_{app} = (k_0 K_{HI} + k C_{b-H})/(K_{HI} + C_{b-H})$$

C_{b-H} : concentration of biotin−heparin.

After rearrangement, k_{app} can expressed as

$$k_{app} = -K_{HI}(k_{app} - k_0)/C_{b-H} + k.$$

K_{HI} and k can be determined using experimentally determined k_{app} values obtained at the corresponding C_{b-H} values, through plotting k_{app} vs. $(k_{app}-k_0)/C_{b-H}$. The two variables, k_{app} and $(k_{app}-k_0)/C_{b-H}$, were found to be linearly correlated with calculated values for K_{HI} and k of $(2.30\pm0.55)\times10^{-7}$ M and k $(2.42\pm0.17)\times10^9\,M^{-1}\,min^{-1}$, respectively. In the absence of heparin, k_0 ($= k_{app}$) is $2.2\times10^6\,M^{-1}\,min^{-1}$, which is three orders of magnitude less than k. Good correlation between the kinetic model and experimental data suggests that in a range of heparin concentration between 1 nM and 1 μM, heparin-accelerated thrombin inactivation is indeed a two-step mechanism, which includes the rapid formation of a heparin–ATIII inhibitory complex that subsequently reacts with free thrombin. The reaction occurs more rapidly than that of the free ATIII and thrombin in the absence of heparin. Of interest, little difference was noted between K_{HI} and k values obtained from our investigation of biotinylated heparin and those reported in other studies of heparin alone (Table 3).

3.2. Determination of heparin surface density

A mixture of ^{3}H-heparin and unlabeled heparin was biotinylated. The extent of biotin derivatization was 0.975 ± 0.025 mol biotin/mol heparin and the specific activity of the mixed system was 324.6 cpm/μg. A heparinized surface was fabricated by anchoring the compound on a SA-coated membrane-mimetic surface.

Table 3
Comparison of heparin–antithrombin dissociation (K_{HI}) and second-order rate constants (k) from the current and previous studies

	K_{HI} (M)	k ($M^{-1}\,min^{-1}$)
Maaroufi et al. [9] (UFH[1])[a]	3.7×10^{-7}	1.3×10^{9}
Jordan et at. [27] (LMWH[2])[b]	1.0×10^{-7}	1.9×10^{9}
Olson [39] (LMWH[3])[b]	2.3×10^{-7}	N/A
Griffith [7,24] (UFH[1])[b]	1.0×10^{-7}	N/A
Current study	2.3×10^{-7}	2.4×10^{9}

1. UFH (unfractionated heparin,): Mw~15 kDa.
2. LMWH (low molecular weight heparin): Mw~6.5 kDa.
3. LMWH: ~8 kDa.
a. K_{HI} was computed from experimental data.
b. K_{HI} was determined directly from the change in the intrinsic fluorescence of AT observed during the formation of the heparin–ATIII complex.

Table 4
Heparin surface concentration as a function of the biotin mole fraction in a membrane-mimetic thin film

Biotin mole fraction	b–heparin ($pmol/cm^2$)[a]
2	1.93 ± 0.26
5	3.47 ± 0.41
10	4.36 ± 0.44
20	5.34 ± 0.51
50	5.94 ± 0.59

[a]Mean ± standard deviation, $n = 6$.

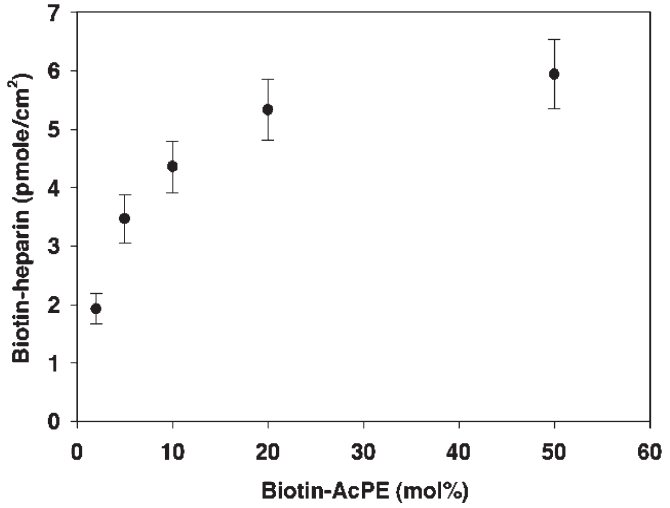

Fig. 6. Surface density of heparin as a function of the mole fraction of biotin in membrane-mimetic thin films. Each data point represents mean ± standard deviation ($n = 6$). Standard error was <10%.

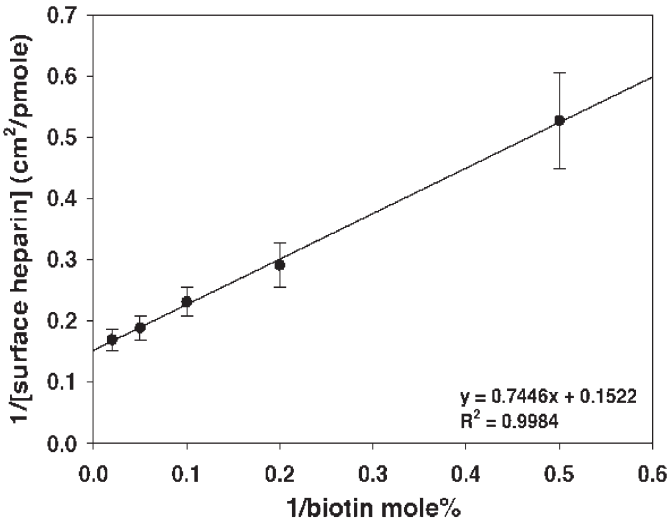

Fig. 7. Lineweaver–Burke plot of biotinylated heparin binding to streptavidin functionalized membrane-mimetic thin films (see data in Fig. 6). The linear relationship is consistent with a binding mechanism that follows a Langmuir binding isotherm. Each data point represents mean ± standard deviation ($n = 6$).

Heparin surface density was a direct function of surface biotin content (mol% of biotin-AcPE) (Table 4). Surface heparin content became saturated when biotin content within membrane-mimetic surface exceeded 50 mol% (Fig. 6). Heparin surface concentration as a function of biotin content within membrane-mimetic construct was expressed in a double reciprocal (Lineweaver-Burke) plot, i.e. 1/[heparin surface concentration] vs. 1/[biotin mol%] and a linear relationship was observed (Fig. 7). From the intercept of the fitted equation, the saturated heparin surface concentration was approximately 6.6 $pmol/cm^2$ or 91.0 ng/cm^2.

Previous studies that have examined the binding kinetics between SA and a biotin-bearing self-assembled monolayer of long chain alkanes [28,29] have revealed that the amount of SA adsorption increases with surface mole fraction of biotin at low surface biotin concentrations, which provides more binding sites for anchoring biotin or biotinylated molecules. SA adsorption approaches a maximum at ~230 ng/cm^2 (~4 $pmol/cm^2$) in the presence of 50 mol% of surface biotin [29]. Thus, the gradual saturation of surface heparin may occur, in part, due to a limit of bound SA. This phenomenon may be a result of the formation of biotin microdomains that we have previously observed with increasing mole fraction of biotinylated lipids [17], and/or steric crowding effects as larger SA molecules bind to the surface [29]. Indeed, it has been observed that saturation coverage of SA decreases at high surface biotin concentrations [29,30].

Given the fact that SA binding to a biotin-containing monolayer normally exposes two of its binding sites away from the surface [30–32], the maximum surface content of biotinylated heparin onto SA-biotinylated membrane-mimetic surface could be, in principle, double the amount of SA surface concentration. However, the accessibility of biotin–heparin to SA binding sites and the potential of competitive desorption of surface SA by biotin–heparin could contribute to lower the maximum surface content of heparin.

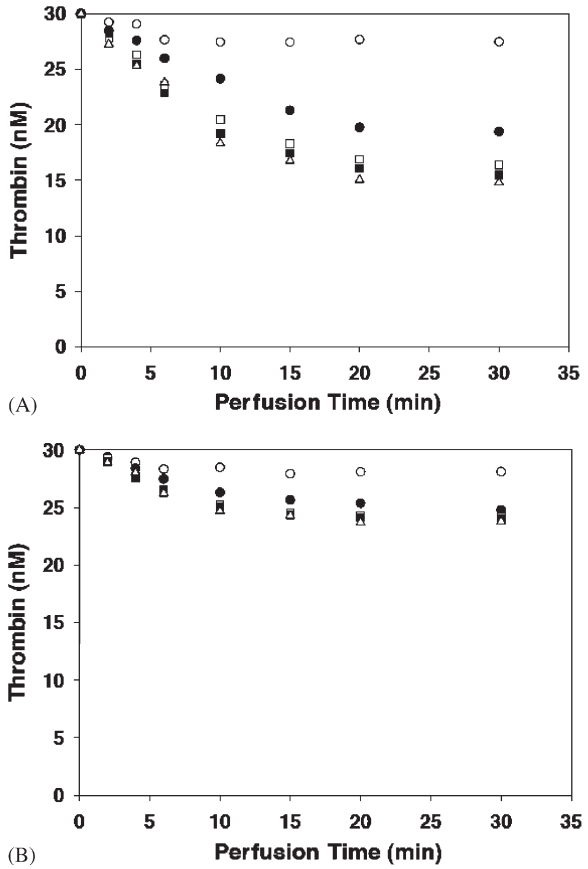

Fig. 8. Thrombin inactivation during the perfusion of thrombin and antithrombin III over surfaces of varying heparin surface concentration: 0 (○), 3.47 (●), 4.36 (□), 5.34 (■), and 5.94 pmol/cm^2 (Δ) at shear rates of 50 s^{-1} (A) and 500 s^{-1} (B). Each data point represents a mean value ($n = 4$). Standard error was <10%.

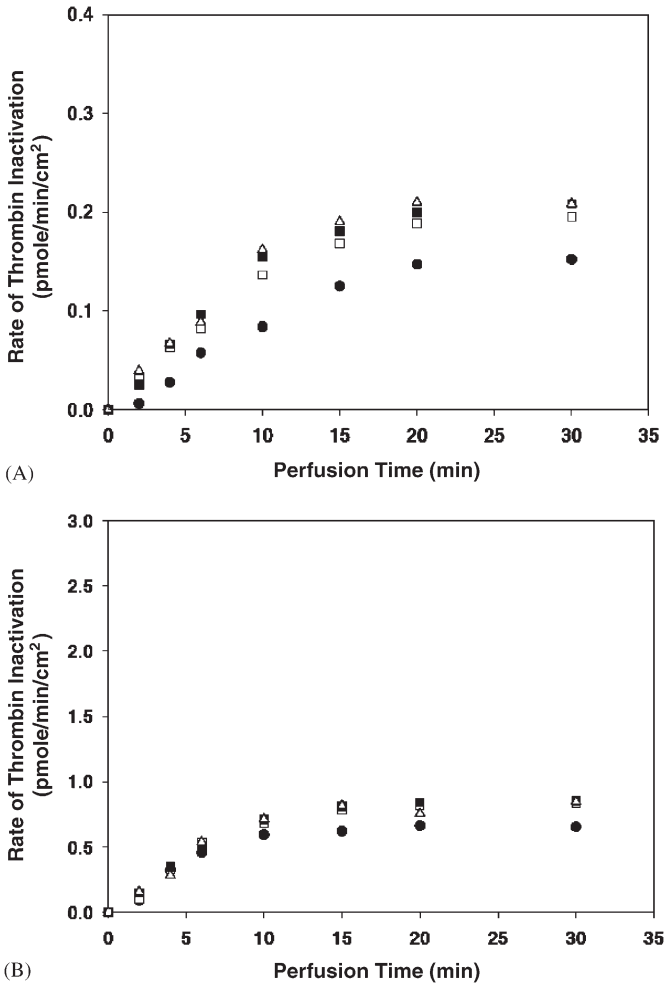

Fig. 9. Rate of thrombin inactivation (level of thrombin decay (pmol/cm^3) × flow rate (cm^3/min)/heparin surface area (cm^2)) at shear rates of 50 s^{-1} (A) and 500 s^{-1} (B) as a function of heparin surface concentration: 3.47 (●), 4.36 (□), 5.34 (■), and 5.94 pmol/cm^2 (Δ). Each data point represents a mean value ($n = 4$). Standard error was <10%.

3.3. The effect of shear regime on the catalytic efficiency of surface bound heparin

Thrombin decay curves in the presence of different surface densities of biotinylated heparin are shown (Fig. 8). In the absence of surface heparin, thrombin levels at both shear rates of 50 and 500 s^{-1} stabilized after 20 min of perfusion. Approximately 1.9–2.5 nM of thrombin was inactivated by fluid phase ATIII, which represents 6–8% of initial thrombin concentration (30 nM). In contrast, in the presence of surface heparin, 35–50% and 15–21% of thrombin was inactivated at shear rates of 50 and 500 s^{-1}, respectively. In addition, time to reach a steady state level of thrombin decay was shorter at higher shear rate (15 min vs 20 min) (Fig. 9). Moreover, our results revealed that a maximum rate of thrombin decay was achieved when surface heparin was equal to or exceeded 4.4 pmol/cm^2 (61 ng/cm^2), which corresponds to immobilization of heparin onto membrane-mimetic thin films containing at least 10 mol% biotin-AcPE. Within the limitations of this in vitro flow system, which does not reflect the dynamic nature of thrombin generation in vivo, these data define a mass transfer limited regime in which the rate of heparin potentiated thrombin inactivation is not enhanced by a further increase in surface heparin density (Fig. 10) [33–36]. Moreover, these data reemphasize the modest impact of surface bound heparin when compared to its effect as a soluble agent and highlight the limitations of antithrombogenic surfaces that are dependent solely on the presence of immobilized heparin.

4. Conclusions

Heparin was chemically modified by conjugation with a biotin spacer group at the terminal position without significantly compromising its catalytic capacity to promote ATIII-mediated thrombin inactivation. Biotinylated heparin was further utilized for fabricating heparinized surface by immobilizing the compound onto SA functionalized membrane-mimetic thin films. Heparin surface density was found to be a function of the mol% of biotinylated lipids within the membrane-mimetic thin film.

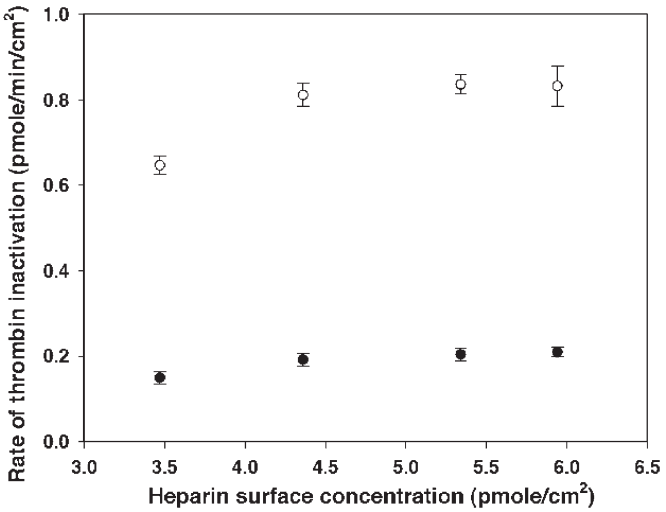

Fig. 10. Steady state rate of thrombin inactivation as a function of heparin surface concentration. Saturated rates of thrombin inactivation were 0.20 ± 0.01 and 0.82 ± 0.03 pmol/min/cm^2 (mean $\pm$ standard deviation) in the presence of surface heparin equal to or greater than 4.4 pmol/cm^2 at shear rates of 50 (○) and 500 (●) s^{-1}, respectively. Data points represent the mean values $\pm$ standard deviation ($n = 4$).

Significantly, surface concentration of heparin increases with increasing surface content of biotinylated lipids until saturation is reached when biotinylated lipids comprise 50 mol% of the total surface lipid content.

In the absence of surface heparin, limited thrombin inactivation by antithrombin was observed at equimolar concentrations of thrombin and ATIII. Although it is anticipated that thrombin inactivation would be higher in the presence of physiologic concentrations of antithrombin (~1.5–2.5 μM) [37,38], the current system illustrates that surface heparin is catalytically active under flow conditions. Moreover, as anticipated, above a specific heparin density the catalytic efficiency of the heparinized membrane-mimetic surface is limited by the transport rates of reactants, i.e. thrombin and antithrombin to the surface in the presence of excess surface heparin. Specifically, under the shear conditions examined, a transport limited heparin surface density was identified at 4.4 pmol/cm^2, which corresponds to 10 mol% of a biotin-containing membrane-mimetic thin film. Inasmuch as membrane-mimetic thin films represent self-assembled systems that can be easily controlled and modified [16–20,22], a platform for creating a robust antithrombogenic environment has been described that is capable of incorporating heparin along with other anticoagulant molecules.

Acknowledgment

Supported by grants from the NIH.

References

[1] Best CH. Preparation of heparin and its use in the first clinical cases. Circulation 1959;19(1):79–86.

[2] Rosenberg RD. Biochemistry of heparin antithrombin interactions, and the physiologic role of this natural anticoagulant mechanism. Am J Med 1989;87(3B):2S–9S.

[3] Bourin MC, Lindahl U. Glycosaminoglycans and the regulation of blood coagulation. Biochem J 1993;289:313–30.

[4] Jordan RE, Oosta GM, Gardner WT, Rosenberg RD. The kinetics of hemostatic enzyme–antithrombin interactions in the presence of low molecular weight heparin. J Biol Chem 1980;255(21):10081–90.

[5] Beeler D, Rosenberg R, Jordan R. Fractionation of low molecular weight heparin species and their interaction with antithrombin. J Biol Chem 1979;254(8):2902–13.

[6] Griffith MJ. Measurement of the heparin enhanced-antithrombin III/thrombin reaction rate in the presence of synthetic substrate. Thromb Res 1982;25(3):245–53.

[7] Griffith MJ. Kinetics of the heparin-enhanced antithrombin III/thrombin reaction. Evidence for a template model for the mechanism of action of heparin. J Biol Chem 1982;257(13):7360–5.

[8] Olson ST, Bjork I. Predominant contribution of surface approximation to the mechanism of heparin acceleration of the antithrombin–-thrombin reaction. Elucidation from salt concentration effects. J Biol Chem 1991;266(10):6353–64.

[9] Maaroufi RM, Jozefowicz M, Tapon-Bretaudiere J, Fischer AM. Mechanism of thrombin inhibition by antithrombin and heparin cofactor II in the presence of heparin. Biomaterials 1997;18(3):203–11.

[10] Mottaghy K, Oedekoven B, Poppel K, Bruchmuller K, Kovacs B, Spahn A, et al. Heparin free long-term extracorporeal circulation using bioactive surfaces. ASAIO Trans 1989;35(3):635–7.

[11] Park KD, Okano T, Nojiri C, Kim SW. Heparin immobilization onto segmented polyurethane-urea surfaces—effect of hydrophilic spacers. J Biomed Mater Res 1988;22(11):977–92.

[12] Nojiri C, Okano T, Park KD, Kim SW. Suppression mechanisms for thrombus formation on heparin-immobilized segmented polyurethane-ureas. ASAIO Trans 1988;34(3):386–98.

[13] Ebert CD, Lee ES, Kim SW. The antiplatelet activity of immobilized prostacyclin. J Biomed Mater Res 1982;16(5):629–38.

[14] Byun Y, Jacobs HA, Kim SW. Binding kinetics of thrombin and antithrombin III with immobilized heparin using a spacer. ASAIO J 1992;38(3):M649–53.

[15] Byun Y, Jacobs HA, Kim SW. Heparin surface immobilization through hydrophilic spacers: thrombin and antithrombin III binding kinetics. J Biomater Sci Polym Ed 1994;6(1):1–13.

[16] Feng J, Tseng P-Y, Faucher KM, Orban JM, Sun X- L, Chaikof EL. Functional reconstitution of thrombomodulin within a substrate-supported membrane-mimetic polymer film. Langmuir 2002;18:9907–13.

[17] Faucher KM, Sun X-L, Chaikof EL. Fabrication and characterization of glycocalyx-mimetic surfaces. Langmuir 2003;19:1664–70.

[18] Chon JH, Marra KG, Chaikof EL. Cytomimetic biomaterials. 3. Preparation and transport studies of an alginate/amphiphilic copolymer/polymerized phospholipid film. J Biomater Sci Polym Ed 1999;10(1):95–107.

[19] Liu H, Faucher KM, Sun X-L, Feng J, Johnson TL, Orban JM, et al. A membrane-mimetic barrier for cell encapsulation. Langmuir 2002;18(4):1332.

[20] Orban JM, Faucher KM, Dluhy RA, Chaikof EL. Cytomimetic biomaterials. 4. In-situ photopolymerization of phospholipids on an alkylated surface. Macromolecules 2000;33:4205.

[21] Marra KG, Winger TM, Hanson SR, Chaikof EL. Cytomimetic biomaterials. 1. In-situ polymerization of phospholipids on an alkylated surface. Macromolecules 1997;30:6483–7.

[22] Sun X-L, Liu H, Orban JM, Sun L, Chaikof EL. Synthesis and terminal functionalization of a polymerizable phosphatidylethanolamine. Bioconjug Chem 2001;12(5):673–7.

[23] Green NM. Spectrophotometric determination of avidin and biotin. Methods Enzymol 1970;18A:418.

[24] Griffith MJ. The heparin-enhanced antithrombin III/thrombin reaction is saturable with respect to both thrombin and antithrombin III. J Biol Chem 1982;257(23):7360–5.

[25] Pletcher CH, Nelsestuen GL. The rate-determining step of the heparin-catalyzed antithrombin/thrombin reaction is independent of thrombin. J Biol Chem 1982;257(10):5342–5.
[26] Lindhout T, Blezer R, Schoen P, Willems GM, Fouache B, Verhoeven M, et al. Antithrombin activity of surface-bound heparin studied under flow conditions. J Biomed Mater Res 1995;29(10): 1255–66.
[27] Jordan RE, Oosta GM, Gardner WT, Rosenberg RD. The binding of low molecular weight heparin to hemostatic enzymes. J Biol Chem 1980;255(21):10073–80.
[28] Jung LS, Shumaker-Parry JS, Campbell CT, Yee SS, Gelb MH. Quantification of tight binding to surface-immobilized phospholipid vesicles using surface plasmon resonance: binding constant of phospholipase A2. J Am Chem Soc 2000;122:4177–84.
[29] Jung LS, Nelson KE, Campbell CT, Stayton PS, Yee SS, Luna VP, et al. Surface plasmon resonance measurement of binding and dissociation of wild-type and mutant streptavidin on mixed biotin-containing alkylthiolate monolayers. Sensor Actuator 1999;B54: 137–44.
[30] Spinke J, Liley M, Schmitt FJ, Guder JH, Angermaier L, Knoll W. Molecular recognition at a self-assembled monolayers: optimization of surface functionalization. J Chem Phys 1993;99(9):7012–9.
[31] Spinke J, Liley M, Guder JH, Angermaier L, Knoll W. Molecular recognition at self-assembled monolayers: the construction of multi-component multilayers. Langmuir 1993;9(7):1821–5.
[32] Knoll W, Angermaier L, Batz G, Fritz T, Fujisawa S, Furuno T, et al. Supramolecular engineering at functionalized surfaces. Synth Metals 1993;61(1–2):5–11.
[33] Kobayashi T, Laidler KJ. Theory of the kinetics of reactions catalyzed by enzymes attached to membranes. Biotechnol Bioeng 1974;16(1):77–97.
[34] Laidler KJ, Bunting PS. The kinetics of immobilized enzyme systems. Methods Enzymol 1980;64:227–48.
[35] Gemmell C, Nemerson Y, Turitto V. The effects of shear rate on the enzymatic activity of the tissue factor-factor VIIa complex. Microvasc Res 1990;40(3):327–40.
[36] Gleason NJ, Carbeck JD. Measurement of enzyme kinetics using microscale steady-state kinetic analysis. Langmuir 2004;20(15): 6374–81.
[37] Griffith MJ, Carraway T, White GC, Dombrose FA. Heparin cofactor activities in a family with hereditary antithrombin III deficiency: evidence for a second heparin cofactor in human plasma. Blood 1983;61(1):111–8.
[38] Murano G, Williams L, Miller-Andersson M, Aronson DL, King C. Some properties of antithrombin-III and its concentration in human plasma. Thromb Res 1980;18(1–2):259–62.
[39] Olson ST. Transient kinetics of heparin-catalyzed protease inactivation by antithrombin III. Linkage of protease-inhibitor-heparin interactions in the reaction with thrombin. J Biol Chem 1988;263(4):1698–708.